Volume 17
Number 33
7 September 2025
Pages 6557–6732

Analytical Methods

rsc.li/methods

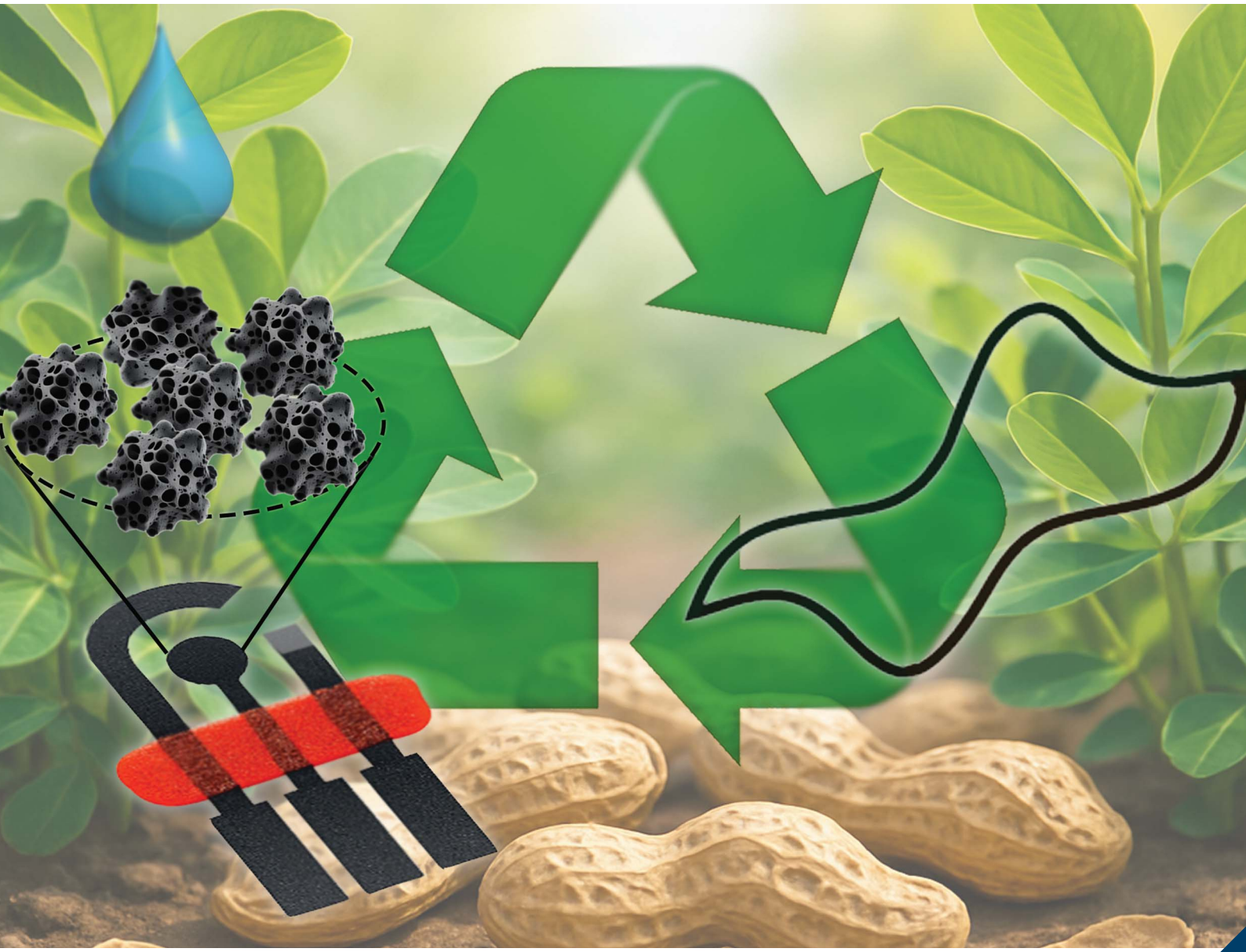

ISSN 1759-9679

ROYAL SOCIETY OF CHEMISTRY

PAPER

F. Bernassani, M. Mosquera-Ortega, I. Sánchez, S. Susmel, E. Cortón and F. Figueredo
Sustainability from the start: biochar-based conductive inks enable the streamlined fabrication of green electroanalytical devices

Analytical Methods

ROYAL SOCIETY OF CHEMISTRY

PAPER

View Article Online
View Journal | View Issue

Cite this: *Anal. Methods*, 2025, **17**, 6565

Sustainability from the start: biochar-based conductive inks enable the streamlined fabrication of green electroanalytical devices†

Florencia Bernassani, [a] Monica Mosquera-Ortega, *[bc] Ismael Sánchez, [a] Sabina Susmel, [b] Eduardo Cortón [a] and Federico Figueredo [a]

The design of low-cost and disposable printed electrodes (PEs) has garnered significant attention from the scientific community in recent years. It is crucial to achieve industrial scalability by addressing the cost of conductive inks and ensuring their environmentally friendly disposal. The utilization of biochar, a carbon-rich material derived from the pyrolysis of biomass waste, represents a promising and sustainable alternative to conventional carbon sources. In this study, peanut shell biochar produced with a low-cost pyrolytic kiln reactor was incorporated into conductive inks. As far as we know, biochar-based ink was used to fully fabricate stencil-printed electrodes for the first time. Three different chemical treatments were employed to activate the biochar and enhance its properties. XPS analysis and electrochemical characterization studies showed that organic solvents improved the characteristics of the biochar when compared to acid or alkaline activation treatments. As a proof of concept, the electrodes were used to detect paracetamol as a model analyte for emerging environmental contaminants. An analytical greenness metric (AGREE) was used to infer how environmentally friendly the analytical procedure is, yielding an overall score of 0.72, which indicates a high degree of environmental sustainability. This study underscores the importance of implementing simple strategies to obtain cost-effective PE, thereby promoting green analytical methods using recycled materials such as bio-waste-derived biochar. This approach may reduce dependence on non-environmentally friendly materials for sensor fabrication and contribute to addressing industrial waste recycling challenges.

Received 1st May 2025
Accepted 30th June 2025

DOI: 10.1039/d5ay00740b

rsc.li/methods

1. Introduction

The development of miniaturized technologies has led to remarkable progress in the analytical chemistry field. The recent development of portable and low-cost potentiostats enables the use of precise electroanalytical sensors outside of traditional laboratory settings. The use of portable, battery-powered and wireless potentiostats that could be integrated with Internet of Things (IoT) technology is of high interest. Wireless potentiostats connected to a smartphone using Wi-Fi or Bluetooth were recently used to perform on-site analysis.[1–4] This positions electrochemical sensors as a powerful bridge between analytical research and in-field sensing applications, especially in decentralized or resource-limited settings.

Along with the development of portable potentiostats, there have been significant advances in portable and disposable single use electrochemical cells. Printed electrodes are disposable sensors that can be fabricated *via* screen-, stencil-, pad- and inkjet-printed methods, or by direct approaches based on drawing or immersion techniques.[5–7] The production and use of printed electrodes is questioned as they are supposed to be disposable and designed for single-use analytical purposes. In general, printed electrochemical cells and electrodes generate considerable amounts of electronic waste (e-waste), which is often discarded in landfills, posing potential health and environmental risks. To fabricate a conventional carbon-based electrochemical cell, the carbon layer is usually printed above a silver track. Silver-based formulations continue to be the predominant materials used to ensure low resistance and high electrical conductivity. However, they present serious limitations, including non-biodegradability, difficulties in recycling, and concerns related to environmental and health toxicity.[8] Additionally, most of the ink formulations (carbon, silver and others) rely on organic solvents and polymeric binders, which also pose an environmental risk due to the release of volatile

[a]*Laboratorio de Biosensores y Bioanálisis (LABB), Departamento de Química Biológica e IQUIBICEN – CONICET, Facultad de Ciencias Exactas y Naturales, Universidad de Buenos Aires (UBA), Ciudad Autónoma de Buenos Aires, Pabellón 2, Ciudad Universitaria, Argentina*

[b]*BioAnalytical Chemistry Lab, Department of Agri-food, Environment and Animal Sciences (Di4A), University of Udine, Udine, Italy. E-mail: monica.mosquera@uniud.it*

[c]*Basic Science Department, Mechanical Engineering Department, Faculty Regional General Pacheco, National Technological University, Argentina*

† Electronic supplementary information (ESI) available. See DOI: https://doi.org/10.1039/d5ay00740b

and organic compounds that contribute to environmental pollution.[9] Recent advances in printed electrodes have incorporated engineered nanomaterials, such as metal oxides and synthetic polymers, to enhance electrochemical performance. It is widely recognized that these materials may be released into the environment through their synthesis, transportation, utilization, and disposal processes, potentially impacting both human health and the environment. Although some risk assessments have been conducted, the widespread use of nanoparticles in disposable electronics remains uncertain.[10] Furthermore, although carbon materials are acknowledged for their low toxicity, the production process involves substantial energy consumption and the use of non-renewable fossil fuels, which significantly contribute to the carbon footprint and the overall environmental pollution.[11] In this context, the development of green and more sustainable materials for the fabrication of printed electrodes is becoming a priority.[12,13] Many researchers are exploring new fabrication strategies and materials to develop more sustainable electroanalytical devices. Among these strategies, researchers are seeking new sustainable materials for the development of conductive and low environmental impact inks.[13] Advances in this field have also been made using various binder materials, such as ethyl cellulose, polymeric resins, glass varnish and glue, among others.[14–18] The catalyst material plays a significant role not only in electrochemical performance but also in the sustainability. A new trend in electrochemistry involves the use of materials considered green, such as biochar. Biochar is a carbon-rich bio-based material produced through the pyrolysis or carbonization of biomass or sludge in a low-oxygen atmosphere.[12] Various types of biomass feedstock, in general derived from waste, could be valuable for producing biochar. Peanut shells are an example; this is an agricultural by-product, accounting for around 30% of the total weight of peanuts. Around 11 million tons of this material are generated globally each year, and a significant amount of it is discarded without further use.[19] Due to their low density and high volume, peanut shells present challenges in terms of disposal and management. However, their rich composition of lignin, cellulose and hemicellulose makes them resistant to rapid environmental degradation.[20] These characteristics make peanut shells an attractive raw material for producing biochar[21] which has a variety of applications, ranging from soil and water remediation to the development of electrode materials. In particular, biochar-derived electrodes have shown promise for electrochemical applications, including the detection and identification of environmental pollutants,[22] and have shown more significant environmental and economic advantages over other carbonaceous materials, such as graphite.[23,24] Despite the advantages of biochar in electroanalysis, its properties can vary greatly depending on the type of source and pyrolysis conditions. These differences affect conductivity and surface chemistry, resulting in significantly different electrochemical behaviors. As a result, it is still challenging to develop standard protocols for biochar-based sensors.[25]

In the field of electroanalysis, biochar has garnered notable interest not only for being a recyclable material but also for its intrinsic characteristics, including a large surface area, porosity, high levels of functionalization, biocompatibility and natural absorptive properties.[26] Furthermore, specific functional groups or metals could be incorporated into the carbon lattice through chemical processes, enhancing selectivity, sensitivity, and catalytic efficiency.[27] As an electrochemical sensor, biochar was used as a modifier for carbon paste electrodes (CPE)[22] or for the surface modification of screen-printed electrodes (SPEs) using drop-casting methods, achieving successful results in detecting metal traces (such as Pb and Cd, among others), pesticides, pharmaceutics and caffeine.[18,28–30] Recently, Gemeiner *et al.*[18] screen printed a biochar layer over a previously printed carbon track, demonstrating a promising alternative to conventional drop-casting methods for electrode modification. Furthermore, Fiori *et al.*[31] recently published fabricated whole cell electrochemical sensors utilizing the stencil printing method, except for the working electrode, which was prepared using biochar inks deposited by vacuum filtration. Interesting advances in the development of biomass-derived carbon materials was made by You *et al.*[32] The authors synthesized biomass-derived graphite from biochar that was later exfoliated to produce bio-graphene inks, and then used to produce a screen-printed film. Interestingly, the conductivities obtained were comparable to those obtained with natural graphite.

Acetaminophen (paracetamol) is an OTC (over-the-counter) drug with a strong analgesic and antipyretic effect. Increasing usage and incorrect disposal of this pollutant have led to its entry into the environment and have become an important water resource contaminant.[33] This compound has been identified in multiple environmental media, such as drinking water, surface water, and wastewater. This is an ecological threat that will endanger both human health and aquatic systems.[34,35] A mega-study conducted by Wilkinson *et al.*[36] in 2022 revealed that one of the most heavily contaminated regions is situated in South America, attributed to inadequate wastewater and waste management infrastructure. In South America, a concentration value of 7.58 $\mu g\ L^{-1}$ has been established, whereas for Argentina, it stands at 4.90 $\mu g\ L^{-1}$. Nonetheless, the highest recorded concentration of 227 $\mu g\ L^{-1}$ was identified at a site along the Seke River in La Paz, Bolivia, resulting from direct discharges from septic tanks and solid waste.[36] In consideration of these findings, there is a need for accurate, rapid, and low-cost drug contamination analysis for understanding drug pollution and developing appropriate solutions. In these circumstances, electrochemical detection systems have emerged as a very attractive alternative for paracetamol detection in aqueous media.[37]

Although there have been reports of the fabrication of biocarbon-based electrodes by several authors,[18,22] in this work there is a highlighting of the single-stage fabrication using the disposable electrode stencil technique. Biochar was activated, and ink composition was optimized to enhance the electrochemical performance. As a proof of concept, the PEs obtained were used to detect an emerging environmental contaminant model analyte such as paracetamol. Finally, an assessment of analytical methodology greenness – AGREE metric system tool – was performed.

2. Materials and methods

2.1. Materials

Biochar (BC) derived from peanut shells (a local producer) was obtained by means of a home-kiln system without control of temperature and pressure during carbonization, according to Long and Arnal *et al.*[38] Graphite (Gr) was purchased from Grafitos Coloidales Juan Carlos Espiñeira Loeda. Vulcan XC-72 carbon black (CB) was acquired from Fuel Cell Store. Nail polish was obtained from a local producer. Acetone, potassium chloride, potassium hydroxide, nitric acid (concentrated), and potassium ferricyanide of analytical grade were purchased from Sigma-Aldrich, Argentina. Paracetamol was purchased in syrup form (Termofren, Roemmers S.A.I.C.F, Argentina). Paracetamol stock solution (13.2 mM) was prepared by diluting paracetamol in phosphate buffer (0.1 M, pH 7.2) and stored at 4 °C. All solutions were prepared with Milli-Q water.

2.2. Biochar activation treatments

The removal of aromatic hydrocarbons was performed by organic solvent wash according to a previously published protocol.[39] 1 g of BC was added to 75 mL of acetone and stirred at 1000 rpm for 1 h. Then, the suspension was filtered in a vacuum system and dried at 80 °C for 12 h. After it dried, the obtained powder was ground and sieved with a 53-micron mesh. BC washed with acetone will be referred to as BC_{OS}.

Alkali treatment for BC activation was conducted following a protocol adapted from Huggins *et. al*.[40] 300 mg of BC was immersed in 50 mL of potassium hydroxide (3 M) and heated to 80 °C for 2 h under constant stirring. The content was then filtered through a fritted glass funnel. To eliminate the remaining potassium hydroxide, the powder was washed with water until a neutral pH was achieved. The powder obtained was dried at 80 °C for 12 h. The resulting biochar activated in an alkaline medium will be referred to as BC_{AL}.

Acidic treatment was based on a modified protocol from Oliveira *et.al*.[41] BC (300 mg) was immersed in 50 mL of nitric acid (5 M). The suspension was heated under reflux at 60 °C for 3 h. Then, the suspension was filtered through a fritted glass funnel and washed with distilled water until a neutral pH was reached. The obtained powder was dried at 80 °C. The biochar activated with acid will be referred to as BC_{AC}.

2.3. Physicochemical characterization

In this study, the morphological characterization of BC powder was performed using an FEI Scios 2 field emission microscope (FESEM) with a Schottky emitter. Specific surface area and pore size distribution of BC, BC_{AL} and BC_{AC} were acquired by nitrogen desorption/adsorption measurements (ASAP2020, Micromeritics, USA) using the Brunauer–Emmett–Teller (BET) technique.[42] Elemental analysis of new materials was carried out by X-ray photoelectron spectroscopy (XPS, SPECS Flexmod, Germany) using a monochromatic Al Kα X-ray source (1486.61 eV), 100 W potency, a spot size of 3.5 × 1 mm^2 and a potential difference of 10 kV. Functional group characterization was carried out by using Fourier transform infrared spectra (FTIR) in attenuated total reflectance mode (ATR) (Thermo Scientific Nicolet IS50 FTIR, Madison, WI, EE. UU.) in the range of 400–4000 cm^{-1} with the maximum resolution set at 4 cm^{-1}.

2.4. Stencil printed electrode fabrication

The ink was prepared by adding 300 mg of carbon powder (Table 1) to 300 mg of nail polish. Five hundred microliters (500 μL) of acetone were added to achieve less viscous ink. The stencil-printed electrodes were prepared by applying the conductive ink onto PET that featured an adhesive glossy mask with the cutout for the three-electrode system (working electrode geometric area of 0.125 cm^2), which was delimited using a cutting printer (Silhouette model Cameo 4). The ink was deposited onto the adhesive masks and spread with a squeegee in a single direction. Immediately afterward, the masks were removed, and the printed electrodes were allowed to dry for 24 hours at room temperature. The reference electrode was produced by brushing with Ag flake ink (Electroquímica Delta S.R.L., Argentina), followed by a drop of bleach to generate an Ag/AgCl interface. Subsequently, the detection area was delimited using nail polish. The scheme showing the electrode fabrication is illustrated in Fig. 1.

2.5. Electrochemical characterization

Electrochemical measurements were conducted using a Gamry Interface 1010 B potentiostat (Gamry, Warminster, PA, USA). For this purpose, 200 μL of a 5 mM potassium ferricyanide solution in KCl (0.1 M) was placed in the detection area. The detection and quantification of paracetamol was performed with a Rodeostat Open Source Potentiostat (Model RSTAT-01), a low-cost and portable instrument. Electrochemical impedance spectroscopy was conducted using in a Palm Sens 4 potenciostat (PalmSens BV, Netherlands) using 5 mM of ferricyanide and ferrocyanide ($[Fe(CN)_6]^{3-/4-}$) solution in KCl (0.1 M) with the frequency ranging from 100 kHz to 0.1 Hz, at an amplitude of 10 mV *vs.* OCP.

3. Results and discussion

3.1. Physicochemical characterization

The morphological structure of BC is observed in the SEM micrograph presented in Fig. 2, characterized by the presence of heterogeneous pores, both in shape, including circular, oval, and even amorphous morphologies, and in size, with diameters

Table 1 Weight percentage of conductive powders used to prepare the inks[a]

SPE	Gr (%wt)	BC_X (%wt)	CB (%wt)
Control	85	0	15
BC_X10	75	10	15
BC_X15	70	15	15
BC_X25	60	25	15
BC_X50	35	50	15

[a] X: OS, AL or AC.

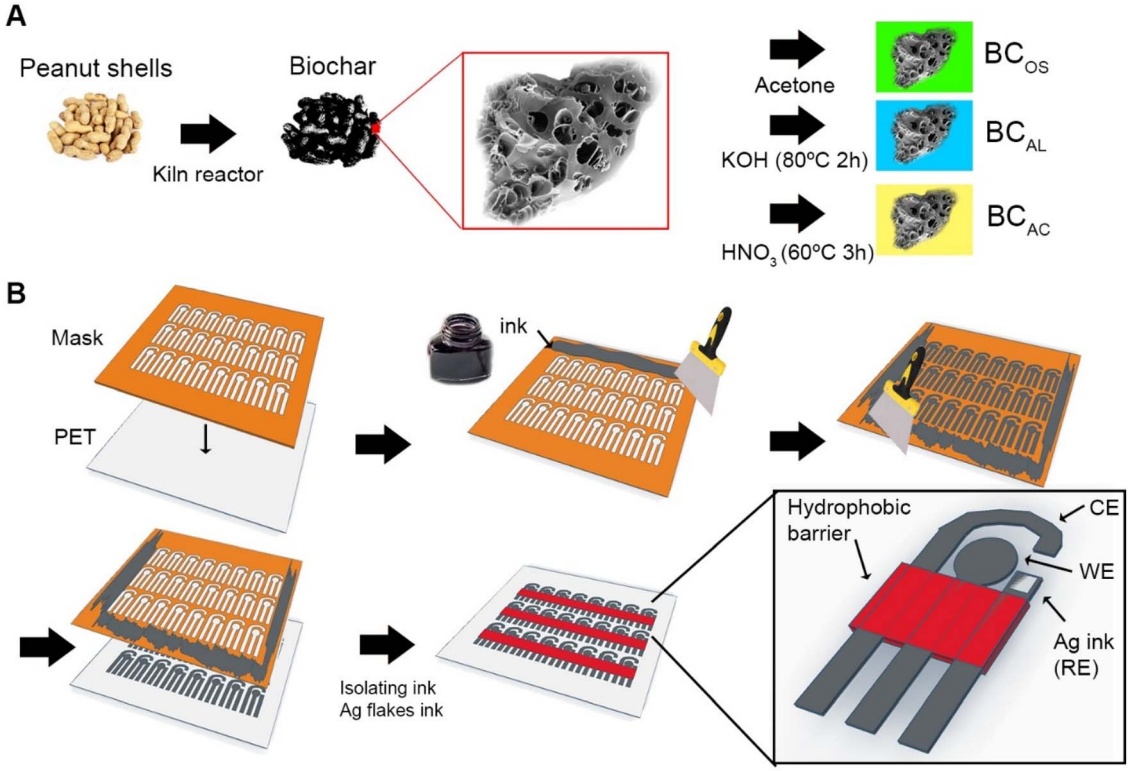

Fig. 1 Fabrication process of PEs. (A) Scheme showing in brief the process to obtain pristine and activated BC. (B) Methodological procedure to obtain the handmade 3-electrode PEs.

ranging from approximately 7 μm to 1 μm. This porosity indicates a significant increase in specific surface area, a phenomenon typically associated with pyrolysis processes conducted at temperatures above 450 °C.[43]

As a complement to the morphological analysis of the porosity of BC, BC_{AL}, and BC_{AC} biochars, nitrogen adsorption was characterized using the BET method (Fig. S1 and Table S1†). The isotherms obtained show that at low relative pressures

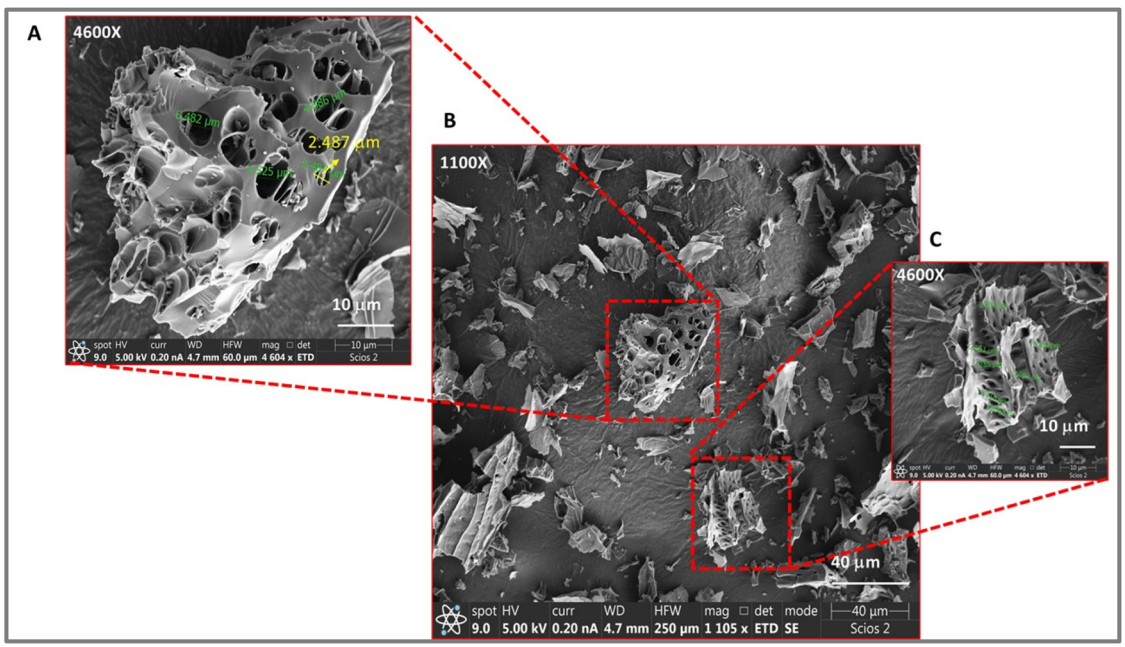

Fig. 2 Morphological characterization of BC powder. SEM micrograph of BC powder after grinding and sieving (53 μm) (A–C) at 1100× (B) and 4600×(A and C).

(P/P_0), the amount of nitrogen adsorbed is limited (BC_{AC} < BC < BC_{AL}), suggesting a low presence of micropores. This observation is consistent with the pore diameters reported in Table S1,† which range from 2.09 to 5.1 nm, corresponding to mesopores according to the IUPAC classification.[44] Additionally, at high relative pressures ($P/P_0 \approx 0.97$), a slight increase in the volume of nitrogen adsorbed is observed in all biochars, which is more pronounced in BC_{AC} (4.6 cm^3 of N_2 adsorbed). This behavior indicates a low mesopore density and the absence of significant microporosity.[45] Together, these features suggest that the materials exhibit a porous structure with moderate adsorption capacity, possibly due to the pyrolysis method used in this work, whose temperature and pressure conditions were not controlled. The above makes this material potentially suitable for functionalization processes aimed at electrochemical applications.

Elemental composition analysis by XPS of BC and its activation products (BC_{AL}, BC_{AC} and BC_{OS}) is shown in Fig. 3. Survey spectra show, in all samples, two predominant peaks corresponding to C at 284.4 eV and to O at 530 eV, and a third weak signal matching N (Table 2). The BC and BC_{OS} samples exhibit similar surface compositions, characterized by a predominance of reduced C with sp^2 hybridization and oxidized C species, representing between 91% and 93% of the total atomic content (Fig. 3a2 and b2). Chemical activation treatments with acids and alkali induce modifications in the elemental composition, demonstrating a decrease in C content and a significant increase in O concentration compared to untreated samples.

Analysis of the high-resolution O 1s region (Fig. 3a2, b2, c2 and d2) reveals four main contributions: carbonyl bonds (C=O) at 531.6 eV, ether or hydroxyl bonds (C–O) at 533.0 eV, and two additional signals at 536.0 eV and 530.0 eV, assigned to carbonate (CO_3^{2-}) groups and metal oxides, respectively. These results confirm that chemical activation promotes surface functionalization, increasing the number of available oxygenated groups (Fig. 3c2), a relevant aspect for applications in adsorption and electrochemistry. Furthermore, analysis of the high-resolution N 1s spectra (Fig. 3a4, b4, c4 and d4) shows three main components: a signal at 406 eV attributed to oxidized N species, such as NO_2 and NO_3^-; a second at 398.6 eV corresponding to pyridine groups; and a third associated with pyrrole species and primary amines (–NH_2). N content in BC_{AC} reaches 2.2%, compared to 0.4% observed in the untreated BC, demonstrating the effective incorporation of N groups into the porous structure of the material because of the chemical treatment. This increase in N functionalization is consistent with what has been previously reported in the literature for materials activated under similar conditions.[46,47] In the P 2p region a minimum signal at 133 eV was observed only in the BC_{OS} and BC samples, which is in accordance with PO_3^{2-} (Fig. S2†).

The FTIR-ATR spectra corroborate and extend the findings obtained from the XPS analysis (Fig. 3). Specifically,

Table 2 Elemental analysis of the BC and its derivatives after chemical activation

Element	BC	BC_{OS}	BC_{AC}	BC_{AL}
Carbon	93.17	91.72	85.62	88.56
Oxygen	6.3	7.62	12.1	10.37
Nitrogen	0.42	0.52	2.28	1.07
Phosphorus	0.11	0.14	ND	ND

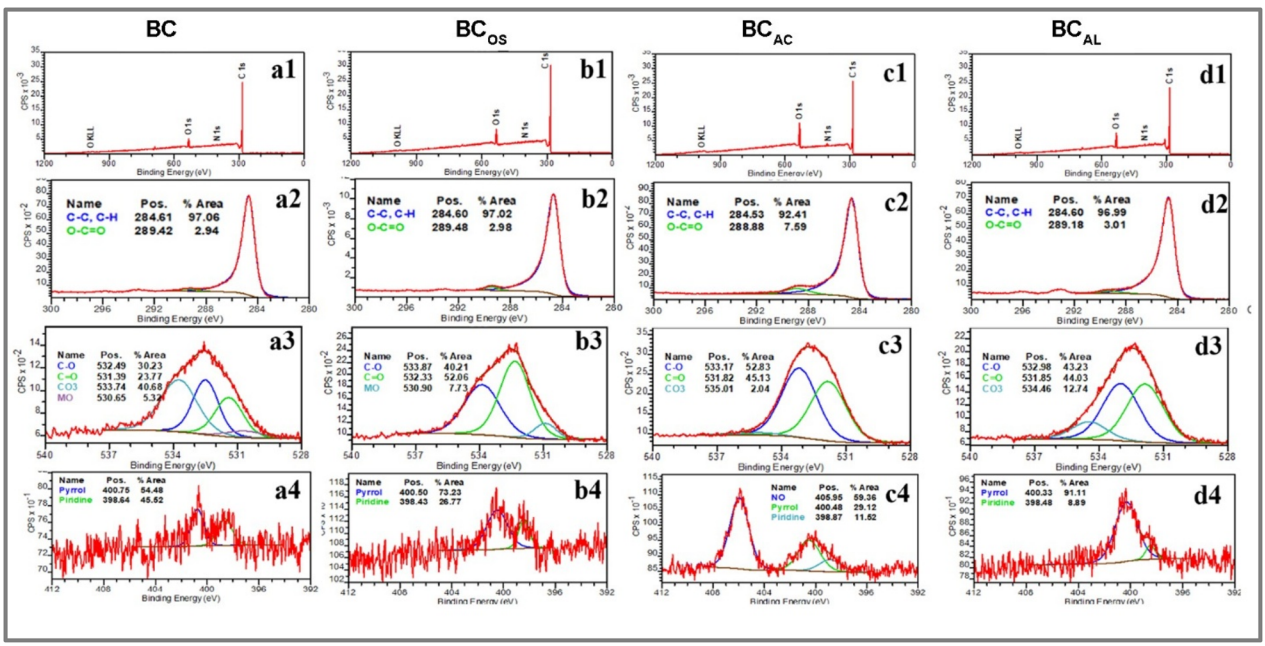

Fig. 3 X-ray photoelectron spectroscopy (XPS) spectra of BC, BC_{OS}, BC_{AC} and BC_{AL}. XPS survey spectra of BC, BC_{OS}, BC_{AC} and BC_{AL} (a1, b1, c1 and d1). In addition, high-resolution spectra of C 1s, (a2, b2, c2, and d2), O 1s (a3, b3, c3, and d3) and N 1s (a4, b4, d4, e4) of diverse biochar materials are presented.

characteristic out-of-plane bending vibrations associated with aromatic C–H bonds were observed in the 600–880 cm^{-1} region. The relative intensity of these signals follows the trend BAL < BOs < BAc < BOS, suggesting differences in the residual aromatic content and degree of structural condensation among the samples. Furthermore, two bands attributable to carbonate ions (CO_3^{2-}) were identified: a bending vibration at approximately 900 cm^{-1} and a stretching vibration at 1459 cm^{-1}. These observations are consistent with the XPS results, where the deconvolution of the C 1s and O 1s spectra revealed contributions corresponding to C=O and O–C=O bonds, particularly in Bc and BAL (Fig. 3a2, a4, d2 and d4), indicative of surface carbonate functionalities. A band associated with the N–O stretching vibration was also detected at 1372 cm^{-1}, with notably higher intensity in the BAC sample. This finding aligns with the high relative content of oxidized nitrogen species (NO_x) identified by XPS for BAC (59.36% of nitrogen-containing groups, Fig. 3c4), supporting the interpretation that BAC underwent a more extensive surface functionalization with nitro or related nitrogen–oxygen groups.

FTIR-ATR and XPS allow us to identify the functional groups present in the biochar and confirm their persistence after the printing process.[22] This information is crucial for understanding the interaction between the modified electrode and analytes such as paracetamol. In this sense, specific interactions (such as hydrogen bonding or charge transfer) can be facilitated by the presence of oxygenated and nitrogenated functional groups, which enhances the sensor sensitivity and selectivity for detection.

3.2. Electrochemical characterization of PEs

The electrochemical response of the fabricated PEs was evaluated *via* cyclic voltammetry (CV) with 5 mM potassium ferricyanide serving as a redox probe. As shown in Fig. 4A, CV curves display the characteristic peaks associated with the ferricyanide/ferrocyanide redox couple. However, as shown in Fig. 4B, the PEs did not exhibit fully reversible behavior; the anodic peaks are always lower than cathodic ones. It was noted that the incorporation of BC into the ink resulted in an increase in the capacitive current. This is very common in biochar, as the porous structure and certain functional groups on the surface promote the formation of a more complex electrical double-charge layer, resulting in an increase in specific capacitance.[26]

Regarding the electrochemical performance, Fig. 4B shows that increasing the proportion of BC up to 15% (BC-15%) resulted in cathodic current peaks comparable to those of the

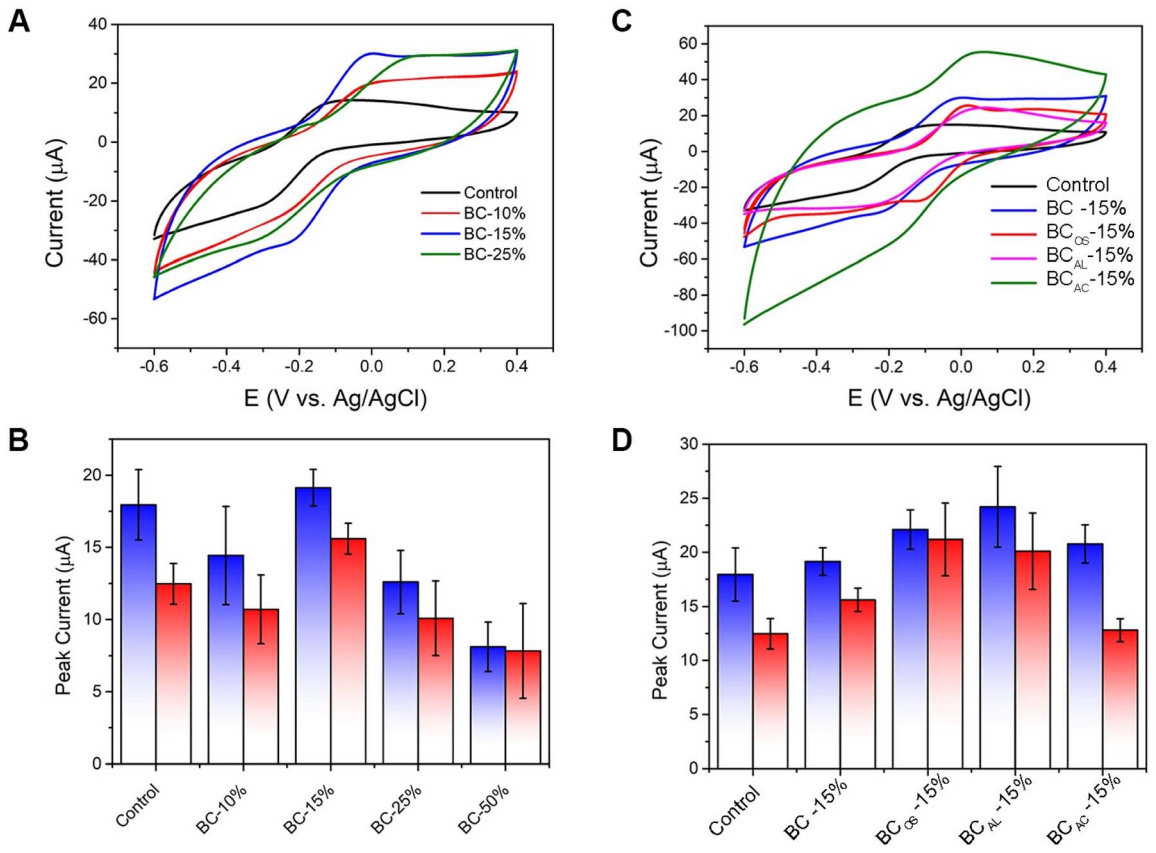

Fig. 4 Electrochemical characterization of PEs: (A) comparative CVs of the control and BC-10, -15, and -25% PEs. CVs were performed in 5 mM ferricyanide in KCl (0.1 M) at a scan rate of 10 mV s^{-1}. (B) Cathodic (blue) and anodic (red) current peaks calculated from the CV curves of A. (C) Comparative CVs of control PEs and those with 15% of pristine and activated BC (BC_{OS}, BC_{AL} and BC_{AC}). Measurements were performed in 5 mM ferricyanide in KCl (0.1 M). (D) Cathodic (blue) and anodic (orange) peak current calculated from the CV curves of C. Error bars indicate the standard deviation (±SD) ($n = 4$).

control electrodes. On the other hand, anodic current peaks of BC-15% were more intense than those of the control, indicating improved electron transfer. Beyond this proportion, for 25% and 50% BC, a reduction in both current peaks was observed, suggesting that 15% of BC represents the optimal composition to prepare the ink.

Activated biochar presents a significant advantage over the precursors in terms of electrochemical performance, particularly in applications such as capacitors, fuel cells, and sensors.[26] This is primarily attributed to the incorporation of functional groups, acid/alkali, or redox reactions of the inherent groups, or by removing undesirable co-products of the carbonization process. To achieve this, three different activation treatments were performed: organic, alkaline, and acidic. Such chemical modifications are commonly made to enhance the biochar adsorptive capacity to further use them to remediate soil and water.[48] Regarding the electrochemical field, these types of activation treatments may enhance the adsorption of ions and molecules, thus facilitating a better contact between the electrode and analyte at the interface, contributing to a better electrochemical performance.[26] In addition, the use of alkali- and acid-treatments could increase the surface area, pore volume and hydrophilicity, which may impact the resulting performance.[49,50]

As shown in Fig. 4C, washing with organic solvent or treating with potassium hydroxide improved the catalytic performance of PEs (BC-15%) by 22% and 33%, respectively, compared to the control PEs. The cathodic currents obtained for the control, $BC_{OS}15\%$, and $BC_{AL}15\%$ were 18 ± 3, 22 ± 2, and 24 ± 3 μA, respectively. For practical purposes, the effect of the activation treatments of BC on the electrochemical performance of PEs was evaluated only in the optimal proportion, BC-15%. The improved performance of $BC_{OS}15\%$ could be related to the loss of absorbed oils from the biochar surface, as was previously demonstrated for other carbon materials.[39] Alkaline treatments are not only useful for removing the oils produced during incomplete combustion but can also react with inorganic compounds such as SiO_2 to form silicates that are easy to remove.[51] Additionally, potassium hydroxide can also neutralize phenolic, lactonic and carboxylic groups present on the surface.[52] In contrast, acid treatment did not present a significant improvement in the catalytic activity ($I_c = 20 \pm 2$ μA), but an increase in capacitance was noted. The latter may be attributed to a sum of effects, seen in the XPS and BET analysis (Fig. S1, S2 and Table S1†), such as an increase in the width of the pores, a higher concentration of acidic functional groups on the surface by oxidation and increased surface defects.[26,53] Furthermore, XPS analysis of the N 1s and O 1s regions corroborates this interpretation (Fig. 3). The BC_{AC} exhibited a high proportion of N-oxide species (59%) in the N 1s spectrum (Fig. 3c4) and an increased content of oxygenated groups (C–O 52.83% and C═O 45.13%) in the O 1s region (Fig. 3c3). These features enhance capacitance through the introduction of redox-active and polar sites but may also generate electron-withdrawing functionalities and acidic sites that hinder efficiency. This is particularly relevant for paracetamol, whose electrochemical oxidation relies on efficient electron transfer to its phenolic group. In contrast, $BC_{OS}15\%$ presented an N 1s spectrum dominated by pyrrolic nitrogen (73%) (Fig. 3b4), which improves electrical conductivity and catalytic activity. It also presented an O 1s profile enriched in carbonyl (C═O 52.06%) and C–O (40.21%) groups, which likely facilitate paracetamol adsorption (Fig. 3b3). It is well established that the ferricyanide/ferrocyanide redox probe is sensitive to the properties of the electrode surface. The presence of deprotonated carboxylic acid functionalities produced after acid treatment may induce electrostatic repulsion between the electrode surface and the negatively charged redox species, thereby adversely affecting the associated electrochemical response.[54] However, it is not the sole explanation possible; acid treatments produce defects in the carbon structure and damage the graphitic network, resulting in a decrease in electrical conductivity, which may directly impact the electrochemical properties.[55]

The reversible behavior of PEs produced in this study was determined after calculation of the peak-to-peak separation (ΔE). The incorporation of BC in the SPE resulted in higher values ($\Delta E_{BC\text{-}15\%} = 234 \pm 20$ mV) with respect to the control ($\Delta E_C = 168 \pm 10$ mV), which may be related to a change in the analyte diffusion within the material electrode or a partial refraining of electron transfer due to the presence of BC. Interestingly, BCos15% presented a lower peak-to-peak value ($\Delta E_{BCOS15\%} = 157 \pm 20$ mV) comparable to the control, reflecting an improvement in the electrode performance. Conversely, alkaline and acidic treatments did not show a significant improvement in reversibility behavior as the values remained like those observed for untreated BC-15% electrodes ($\Delta E_{BCAL15\%} = 242 \pm 32$ mV and $\Delta E_{BCAC15\%} = 223 \pm 22$ mV). While these treatments may enhance the capacitance or current response, they did not improve the reversibility behavior.

Electrochemical impedance spectroscopy (EIS) measurements were conducted using the electrodes control, BC15%, $BC_{OS}15\%$, $BC_{AL}15\%$, and $BC_{AC}15\%$, in the presence of a 5 mM equimolar mixture of ferricyanide and ferrocyanide as the redox probe, as shown in Fig. S3.† According to the literature, the resulting Nyquist plots were fitted using an equivalent circuit based on the Randles model, where the ideal capacitor was replaced by a constant phase element (CPE) to account for the non-ideal capacitive behavior of porous electrodes.[31,56,57]

From the fitted model, the charge transfer resistance (R_{ct} and R_2 in the equivalent circuit model) was extracted and analyzed. The observed R_{ct} values followed the trend $BC_{AL}15\% \approx$ control $<$ $BC_{AC}15\%$ $<$ BC15%. The BC15% electrode showed significantly higher R_{ct} values compared to the control (987.0 Ω *vs.* 242.4 Ω, respectively), suggesting that the incorporation of untreated biochar increases interfacial resistance. A similar trend was observed by Silva *et al.*,[30] who attributed this effect to the amorphous structure of biochar, which impairs efficient charge transport. Interestingly, CV experiments revealed comparable redox peak intensities across most electrodes, indicating that electroactive surface area plays a significant role in the electrochemical response despite variations in R_{ct}. $BC_{OS}15\%$ exhibited a reduction in R_{ct} (391.5 Ω) compared to BC15% (987.0 Ω), consistent with the removal of surface-bound

oils or hydrophobic residues by organic solvent washing, which likely improved electrolyte wetting. $BC_{AL}15\%$ also showed R_{ct} values (209.8 Ω) lower than those of $BC_{OS}15\%$. In contrast, although $BC_{AC}15\%$ exhibited lower R_{ct} (585.3 Ω) than BC15% (987.0 Ω), its CV response was less favourable. This discrepancy may be attributed to surface overoxidation induced by acid treatment, which can negatively affect the electrode/analyte interface by introducing excessive surface functionalities that hinder effective redox interaction, rather than simply altering conductivity.

As a proof of concept, the electrodes developed in this study were used to detect an emerging contaminant such as acetaminophen, also known as paracetamol (PA). The measurements were performed using an Io Rodeo potentiostat, which offers a low-cost alternative, simple hardware and open-source software.[58] Thus, this is a much more portable and cost-effective approach, facilitating the creation of a future on-site sensing system with no requirements for conventional equipment in such a context.

All modified, pristine and treated BC-based electrodes ($BC_X15\%$) were used to detect paracetamol. This selection was made considering that paracetamol is a neutral molecule, in contrast to the previously charged redox probe (ferricyanide), which may interact differently with the electrode surface.

Chronoamperometric (CA) assays were selected due to their rapid response and simplicity in view of future applicability for in-field analysis or for automated sensing systems. Moreover, portable and low-cost potentiostats are not able to perform sophisticated techniques, such as differential pulse voltammetry or square wave voltammetry (SWV), with accuracy or precision comparable to those of benchtop equipment, reinforcing the decision to use CA analysis. The electrochemical parameters used for CA analysis were determined from the cyclic voltammetry experiments performed in the presence of 500 μM of PA (Fig. 5A). A potential of +0.60 V *vs.* Ag/AgCl was selected to oxidize paracetamol at the surface of the electrode.

Furthermore, the optimal time for the analyte accumulation was determined at open circuit potential. Up to 300 seconds, no significant changes in the current were observed (Fig. 5B). This behavior suggests an adsorption-controlled process, where it reaches an equilibrium state and saturates the maximum active sites in this configuration.[53,59] In pursuit of a rapid, reproducible signal and fast analytical response, the PEs remained in contact with the sample for 10 min (600 seconds) to be measured before every CA determination. As shown in Fig. 5C, the current recorded in CA assays shows that $BC_{OS}15\%$ exhibited superior performance compared to the control and other modified PEs in the proposed technique.

Based on previous determinations, $BC_{OS}15\%$ PEs were selected for further experiments. The analytical curve for PA was obtained by varying the concentration of the analyte in the range of 10–500 μM. The chronoamperometric responses obtained with $BC_{OS}15\%$ PEs are illustrated in Fig. 6. As shown in Fig. 6B, the set of evaluated concentrations were within the linear range of detection. As indicated in Table 3, the LOD calculated was 8.1 μM in the linear range of 10–500 μM. While the LOD is higher than that of other disposable electrodes,

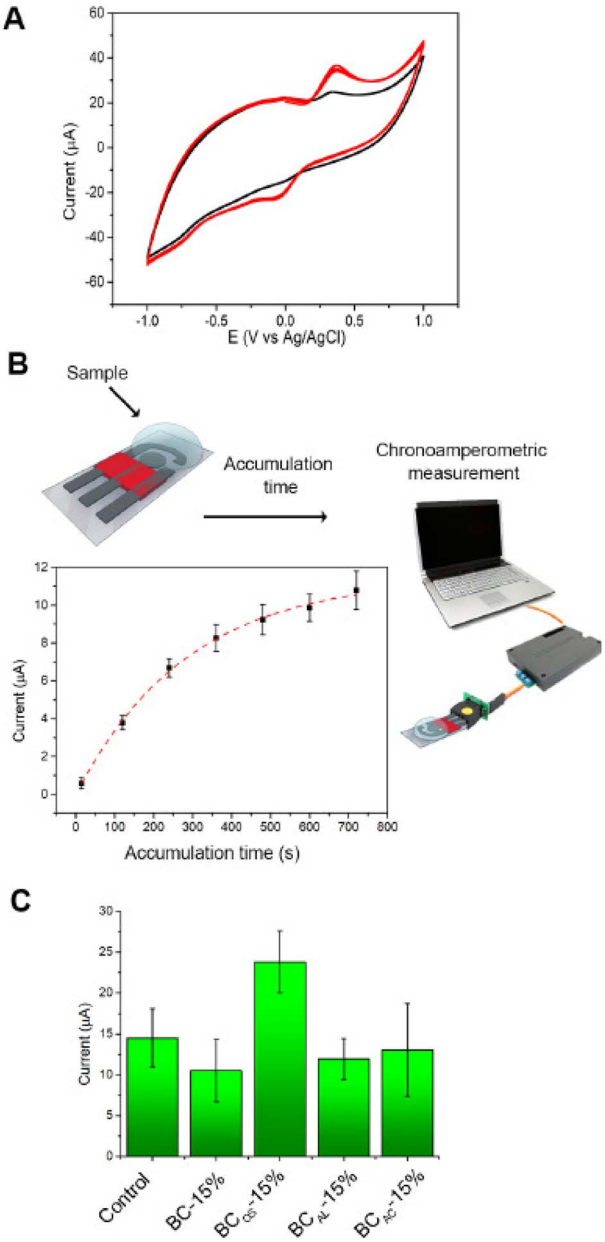

Fig. 5 Optimization experiments for the determination of PA using PEs. (A) CV of $BC_{OS}15\%$ PEs in phosphate buffer (0.1 M, pH: 7.2; black line) containing 500 μM of PA (red line). Scan rate: 10 mV s^{-1}. (B) Current response of $BC_{OS}15\%$ PEs that were in contact with the PA solution for different times before performing the CA assay. (C) Current obtained in CA experiments with 500 μM of PA in phosphate buffer (0.1 M, pH 7.2) after 10 min of pre-concentration. Error bars indicate the standard deviation (±SD) ($n = 4$).

some important considerations should be taken into account. In this work, we employed a Rodeostat potentiostat,[58] which costs approximately USD 200-one of the cheapest commercially available potentiostats in the market. As expected from a low-cost, open-source potentiostat, it lacks some attributes of sophisticated commercial instruments, such as high precision, low background noise, compatibility with very low current measurements, and enhanced robustness. Measuring low

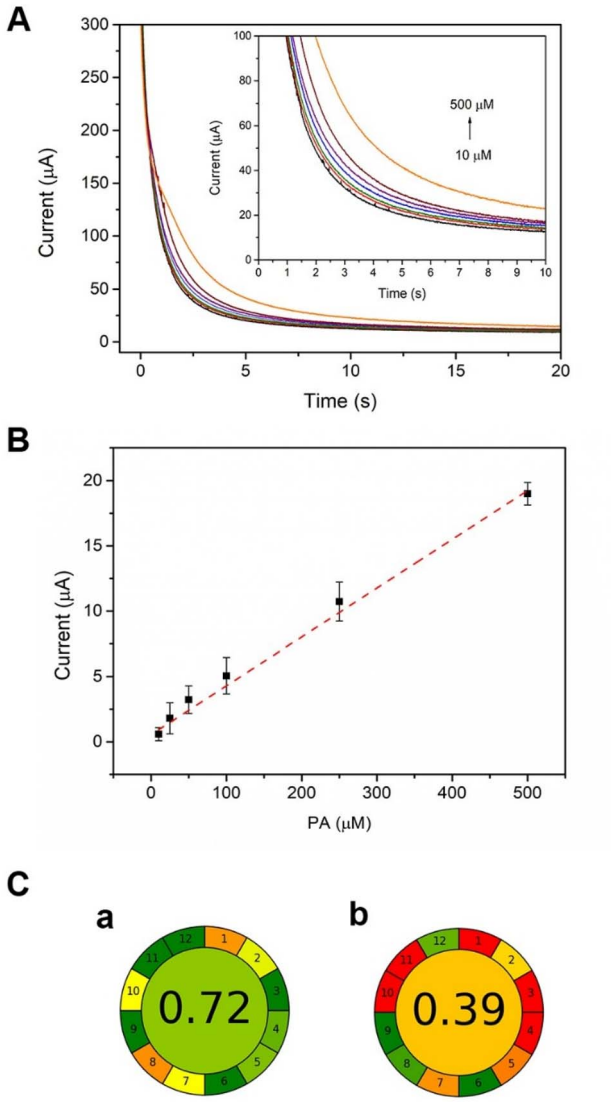

Fig. 6 Analytical determination of PA using BC_{OS}15% PEs and greenness of analytical methodology assessment. (A) CA curves obtained with PA (10, 25, 50, 100, 250, and 500 μM) prepared in phosphate buffer (0.1 M; pH: 7.2). (B) Calibration curve calculated from CA curves. Error bars indicate the standard deviation (±SD) (n = 4). (C) AGREE score and GAC criteria for the analytical method (a) proposed in this study (b) and for a reference method such as HPLC-UV.

currents with minimal noise remains a significant challenge for devices in this class. Consequently, achieving lower LODs compared to high-end commercial equipment is inherently difficult. Furthermore, although CA is a fast and simple technique, other electrochemical techniques, such as SWV, typically offer higher sensitivity and better figures of merit. As this project is still in its early stages, further optimizations will be necessary to enhance sensitivity while maintaining the sustainability and low-cost nature of the method. A distinguishing characteristic of the proposed electrode is its remarkable cost-effectiveness. When aiming for large-scale production of disposable electrochemical cells, screen printing presents a clear advantage over 3D printing in terms of manufacturing speed and scalability. While 3D printing allows for design flexibility and rapid prototyping, it is inherently limited by the relatively slow rate at which individual electrodes can be produced. In contrast, screen printing enables the high-throughput fabrication of electrodes in large batches, making it more suitable for industrial-scale applications where time and cost efficiency are critical.

Determining the greenness of a device or the entire analytical procedure remains a challenge due to its non-well-established methods. Pena-Pereira and colleagues[65] proposed a metric system known as AGREE – Analytical GREEnness – which is an assessment approach to evaluate the greenness of an analytical methodology based on 12 principles of green analytical chemistry (GAC) and transformed into a unified 0–1 scale. The final assessment result combines the individual scores for each principle. The output is a clock-like graph that displays the overall score and color coding at its center. The performance for each principle uses an intuitive red-yellow-green color scale, while the width of each segment indicates the weight of that principle. The assessments were conducted for the proposed and a reference method for detecting paracetamol in aqueous media such as HPLC-UV. As the metric considered the entire analytical procedure, real sample pretreatments as filtration were included in the analysis. For the method proposed here, the metric reaches a score of 0.72 while with HPLC-UV it is 0.34 (Fig. 6C). An overall value close to the ideal value of 1 indicates a high degree of "greenness" compared to the reference analytical methods. In conclusion, according to the principles of green analytical chemistry, the

Table 3 Comparison of different carbon-based disposable electrodes used for the determination of paracetamol[a]

Electrode	Fabrication method	LOD (μM)	Linear range (μM)	Technique	Ref.
CB-PLA	3D printing	0.44	0.4–48	DPASV	60
MWCNT-CB-PLA	3D printing	0.04	5–60	DPV	61
Graphite-PLA	3D printing	0.51	2–100	CV	62
DropSense (110)	Screen printing	0.6	3.3–663	DPV	63
Graphite	Stencil printing	0.2	1–60	CV	64
Biochar/CB/graphite	Stencil printing	8.1	10–500	CA	This study

[a] CB: carbon black. MWCNTs: multiwall carbon nanotubes. PLA: polylactic acid. DPASV: differential pulse anodic stripping voltammetry. DPV: differential pulse voltammetry.

method proposed could be considered greener compared to gold standard methods, despite the relatively high AGREE score obtained for the proposed approach, to acknowledge that not all materials used in the electrode fabrication process align perfectly with green chemistry principles. Herein, nail polish and acetone used for the ink formulation present limitations regarding environmental safety. Nonetheless, further improvements in the fabrication method will be required to obtain more sustainable devices, including cellulose-derived binders or water-based inks based on biodegradable polymers.[18,32] Recently, Camargo *et al.*[9] published an adaptation of the fabrication of screen-printed electrodes to align with sustainable concepts regarding biopolymer binders such as chitosan and PVP, utilizing water as a solvent to eliminate hazardous organic solvents. Additionally, further improvements regarding miniaturization and sensitivity enhancement are necessary to develop a final product with a sustainable perspective and high analytical performance.

4. Conclusion

The development of low-cost, disposable printed electrodes is essential for achieving industrial scalability, particularly by reducing the cost of conductive inks and ensuring environmentally responsible disposal. In this study, we introduced a novel ink formulation incorporating biowaste-biochar, derived from low-cost carbonization, as a sustainable carbonaceous material for printed electrode fabrication. The biochar underwent various chemical activation treatments to enhance its electrochemical performance. Organic solvent washing and alkaline treatment proved to be effective in removing surface oils, increasing surface area and modifying surface chemistry. Paracetamol was selected as a model emerging contaminant to demonstrate its applicability as an electrochemical sensor, and a low-cost, portable potentiostat was employed. The proposed analytical method exhibited a limit of detection of 81 μM, demonstrating its potential for environmental sensing. Despite the need for further optimization to enhance the quality and sensitivity of these printed electrodes, this research lays the basis for the development of a sustainable and accessible electrochemical sensor.

Data availability

The data that support the findings of this study are available from the corresponding author upon reasonable request.

Author contributions

Florencia Bernassani: conceptualization, formal analysis, investigation, methodology, writing – original draft. Monica Mosquera-Ortega: conceptualisation, formal analysis, investigation, methodology, writing – original draft, writing – review & editing. Ismael Sánchez: formal analysis, investigation, methodology, writing – original draft. Sabina Susmel: conceptualisation, writing – original draft. Eduardo Cortón: conceptualisation, funding acquisition, resources, writing – review & editing. Federico Figueredo: conceptualisation, funding acquisition, investigation, methodology, writing – original draft, writing – review & editing.

Conflicts of interest

The authors declare no competing financial interest.

Acknowledgements

This work was supported by the University of Buenos Aires (UBA) and the National Council for Scientific and Technological Research (CONICET). The authors gratefully acknowledge financial support from the National Agency of Scientific and Technological Promotion (ANPCyT) (grant BID-PICT 2020-04023) and from CONICET (grant PIP 2023-0047). The authors acknowledge the Interreg Italy-Croatia Programme 2021-2027 for funding this research, conducted as part of the Standard project BRIGANTINE (ID: ITHR0200237).

References

1 S. C.-H. Lee and P. J. Burke, *Electrochim. Acta*, 2022, **422**, 140481.
2 L. H. B. Vidotto, D. Wachholz Junior and L. T. Kubota, *J. Electroanal. Chem.*, 2023, **937**, 117414.
3 N. F. A. Ibrahim, A. M. Noor, N. Sabani, Z. Zakaria, A. A. Wahab, A. A. Manaf and S. Johari, *HardwareX*, 2023, **15**, e00441.
4 C. Ferreira, F. Barry, M. Todorović, P. Sugrue, S. R. Teixeira and P. Galvin, *Sensors*, 2025, **25**, 762.
5 F. Figueredo, M. Jesús González-Pabón and E. Cortón, *Electroanalysis*, 2018, **30**, 497–508.
6 R. Torre, M. Cerrato-Alvarez, H. P. A. Nouws, C. Delerue-Matos, M. T. Fernández-Abedul and E. Costa-Rama, *Sens. Actuators, B*, 2025, **423**, 136705.
7 S. G. Manjushree and P. S. Adarakatti, *ACS Symp. Ser.*, 2023, **1437**, 1–21.
8 X. Aeby, X. Yan, T. Huber, A. Schneider, G. Siqueira and G. Nyström, *Adv. Mater. Technol.*, 2025, **10**, 2401132.
9 J. R. Camargo, R. D. Crapnell, E. Bernalte, B. C. Janegitz and C. E. Banks, *ACS Appl. Electron. Mater.*, 2025, 7(12), 5599–5610.
10 N. Bisht and P. K. Khanna, *Smart Multifunctional Nano-Inks: Fundamentals and Emerging Applications*, 2023, pp. 413–426.
11 L. Sanchez-Duenas, E. Gomez, M. Larrañaga, M. Blanco, A. M. Goitandia, E. Aranzabe and J. L. Vilas-Vilela, *Materials*, 2023, **16**, 3940.
12 R. D. Crapnell and C. E. Banks, *Green Carbon*, 2023, **1**, 85–93.
13 P. S. Sfragano, S. Laschi and I. Palchetti, *Front. Chem.*, 2020, **8**, 1–7.
14 L. A. Pradela-Filho, I. A. A. Andreotti, J. H. S. Carvalho, D. A. G. Araújo, L. O. Orzari, A. Gatti, R. M. Takeuchi, A. L. Santos and B. C. Janegitz, *Sens. Actuators, B*, 2020, **305**, 127433.
15 L. F. Castro, H. A. Silva-Neto, L. R. Sousa, W. R. de Araujo and W. K. T. Coltro, *Talanta*, 2023, **251**, 123812.

16 L. R. Sousa, H. A. Silva-Neto, L. F. Castro, K. A. Oliveira, F. Figueredo, E. Cortón and W. K. T. Coltro, *Anal. Bioanal. Chem.*, 2023, **415**, 4391–4400.
17 L. F. de Lima, A. L. Ferreira, C. C. Maciel, M. Ferreira and W. R. de Araujo, *Talanta*, 2021, **227**, 122200.
18 P. Gemeiner, O. Sarakhman, M. Hatala, A. Ház, P. Roupcová, T. Mackuľak, J. Barek and Ľ. Švorc, *Electrochim. Acta*, 2024, **487**, 144161.
19 G. Sawargaonkar, R. Pasumarthi, S. Kale, P. Choudhari, S. Rakesh, S. Mutnuri, A. Singh, H. Sudini, M. Ramaraju, R. Singh, A. K. Padhee and M. L. Jat, *Front. Sustain.*, 2024, **5**, 1417207.
20 N. Torres-Lara, A. Molina-Balmaceda, D. Arismendi and P. Richter, *Green Anal. Chem.*, 2023, **6**, 100073.
21 J. L. Zheng, Y. H. Zhu, Y. Y. Dong, Y. Chen and M. Q. Zhu, *Energy*, 2023, **280**, 128223.
22 M. Mosquera-Ortega, F. Figueredo, F. Fernandez, P. Arnal, E. Cortón and S. Susmel, *Carbon Trends*, 2025, **20**, 100520.
23 H. A. Alhashimi and C. B. Aktas, *Resour. Conserv. Recycl.*, 2017, **118**, 13–26.
24 A. T. Ubando, S. C. Ko, W.-H. Chen and S. S. Lam, *Process Saf. Environ. Prot.*, 2025, **198**, 107099.
25 R. Cancelliere, P. Mele, L. Bartolucci, S. Cordiner, W. da Silva Freitas, C. Mazzuca, B. Mecheri, L. Micheli, V. Mulone, E. Paialunga and L. Severini, *J. Environ. Chem. Eng.*, 2025, **13**, 115477.
26 C. Kalinke, P. R. De Oliveira, J. A. Bonacin, B. C. Janegitz, A. S. Mangrich, L. H. Marcolino-Junior and M. F. Bergamini, *Green Chem.*, 2021, **23**, 5272–5308.
27 Y. Zheng, C. Yu and L. Fu, *Green Anal. Chem.*, 2023, **7**, 100081.
28 M. R. Pacheco, S. C. Barbosa, R. F. N. Quadrado, A. R. Fajardo and D. Dias, *Anal. Bioanal. Chem.*, 2019, **411**, 3269–3280.
29 X. Chen, K. Lu, D. Lin, Y. Li, S. Yin, Z. Zhang, M. Tang and G. Chen, *Electroanalysis*, 2021, **33**, 473–482.
30 J. d. O. S. Silva, J. F. dos Santos, H. S. Granja, W. S. Almeida, T. F. L. Loeser, L. S. Freitas, M. F. Bergamini, L. H. Marcolino-Junior and E. M. Sussuchi, *Chemosphere*, 2024, **347**, 140707.
31 S. Fiori, A. Scroccarello, F. Della Pelle, M. Del Carlo, E. Cozzoni and D. Compagnone, *Green Anal. Chem.*, 2025, **13**, 100277.
32 H. You, J. Hui, Y. Zhou, K. Vittore, J. Zhang, L. E. Chaney, S. Chinta, Y. Zhao, G. Lim, D. K. Lee, E. A. Ainsworth, J. B. Dunn, V. P. Dravid, M. C. Hersam and S. J. Rowan, *Small*, 2024, **20**, 2406669.
33 B. Nunes, in *Non-Steroidal Anti-Inflammatory Drugs in Water*, 2020, pp. 131–145.
34 B. M. Al-howri, S. F. Azha, M. S. Shamsudin, N. A. Hamid, A. M. Alsobaai and S. Ismail, *Int. J. Environ. Sci. Technol.*, 2024, **21**, 9743–9762.
35 M. Ortúzar, M. Esterhuizen, D. R. Olicón-Hernández, J. González-López and E. Aranda, *Front. Microbiol.*, 2022, **13**, 869332.
36 J. L. Wilkinson, A. B. A. Boxall, D. W. Kolpin, K. M. Y. Leung, R. W. S. Lai, C. Galban-Malag, A. D. Adell, J. Mondon, M. Metian, R. A. Marchant, A. Bouzas-Monroy, A. Cuni-Sanchez, A. Coors, P. Carriquiriborde, M. Rojo, C. Gordon, M. Cara, C. Moermon and E. Al, *Proc. Natl. Acad. Sci. U. S. A.*, 2022, **119**, e2113947119.
37 A. Miglione, A. Raucci, F. Cristiano, M. Mancini, V. Gioia, A. Frugis and S. Cinti, *Electrochim. Acta*, 2024, **488**, 1–8.
38 L. A. Long and P. M. Arnal, *Chem.: Methods*, 2021, **1**, 477–483.
39 X. Shui, C. A. Frysz and D. D. L. Chung, *Carbon*, 1995, **33**, 1681–1698.
40 T. Huggins, H. Wang, J. Kearns, P. Jenkins and Z. J. Ren, *Bioresour. Technol.*, 2014, **157**, 114–119.
41 P. R. de Oliveira, C. Kalinke, J. L. Gogola, A. S. Mangrich, L. H. M. Junior and M. F. Bergamini, *J. Electroanal. Chem.*, 2017, **799**, 602–608.
42 S. Brunauer, P. H. Emmett and E. Teller, *J. Am. Chem. Soc.*, 1938, **60**, 309–319.
43 G. Sawargaonkar, R. Pasumarthi, S. Kale, P. Choudhari, S. Rakesh, S. Mutnuri, A. Singh, H. Sudini, M. Ramaraju, R. Singh, A. K. Padhee and M. L. Jat, *Front. Sustain.*, 2024, **5**, 1–13.
44 U. Ciesla and F. Schüth, *Microporous Mesoporous Mater.*, 1999, **27**, 131–149.
45 J. Choma, J. Jagiello and M. Jaroniec, *Carbon*, 2021, **183**, 150–157.
46 G. S. dos Reis, D. Bergna, A. Grimm, E. C. Lima, T. Hu, Mu. Naushad and U. Lassi, *Colloids Surf., A*, 2023, **669**, 131493.
47 Z. Wang, X. Pan, S. Kuang, C. Chen, X. Wang, J. Xu, X. Li, H. Li, Q. Zhuang, F. Zhang and X. Wang, *Int. J. Environ. Res. Public Health*, 2022, **19**, 7282.
48 N. Blenis, N. Hue, T. M. C. Maaz and M. Kantar, *Sustainability*, 2023, **15**, 1–15.
49 A. L. T. Zheng, E. T. Y. Lih, Y. P. Hung, S. Boonyuen, S. S. A. O. Al Edrus, E. L. T. Chung and Y. Andou, *Anal. Sci.*, 2025, 1–21.
50 Y. Li, J. Shao, X. Wang, Y. Deng, H. Yang and H. Chen, *Energy Fuels*, 2014, **28**, 5119–5127.
51 H. Huang, J. Tang, K. Gao, R. He, H. Zhao and D. Werner, *RSC Adv.*, 2017, **7**, 14640–14648.
52 L. Tsechansky and E. R. Graber, *Carbon*, 2014, **66**, 730–733.
53 C. Kalinke, P. R. Oliveira, G. A. Oliveira, A. S. Mangrich, L. H. Marcolino-Junior and M. F. Bergamini, *Anal. Chim. Acta*, 2017, **983**, 103–111.
54 M. M. Lounasvuori, M. Rosillo-Lopez, C. G. Salzmann, D. J. Caruana and K. B. Holt, *Faraday Discuss.*, 2014, **172**, 293–310.
55 M. Zhang, M. Yang, M. Yaguchi, H. Jintoku, S. Sakurai and D. Futaba, *Carbon*, 2025, **237**, 120132.
56 Q. Chen, L. Wang, M. He, Y. Wang, D. Bi, J. Huang, C. Wang, X. Xu, Z. Hu and H. Xu, *Electroanalysis*, 2024, 1–16.
57 C. Kalinke, P. R. de Oliveira, M. Bonet San Emeterio, A. González-Calabuig, M. del Valle, A. Salvio Mangrich, L. Humberto Marcolino Junior and M. F. Bergamini, *Electroanalysis*, 2019, **31**, 2238–2245.
58 Io rodeo, Rodeostat: open source potentiostat, **https://iorodeo.com/**, accessed 29 April 2025.

59 M. V. S. Sant'Anna, S. W. M. M. Carvalho, A. Gevaerd, J. O. S. Silva, E. Santos, I. S. C. Carregosa, A. Wisniewski, L. H. Marcolino-Junior, M. F. Bergamini and E. M. Sussuchi, *Talanta*, 2020, **220**, 1–8.
60 J. G. A. Rodrigues, T. M. N. Silva, S. B. Gomes Junior, A. A. L. Marins, G. F. S. dos Santos, R. Q. Ferreira and J. C. C. Freitas, *ACS Omega*, 2025, **7**(12), 1131–1143.
61 R. D. Crapnell, I. V. S. Arantes, J. R. Camargo, E. Bernalte, M. J. Whittingham, B. C. Janegitz, T. R. L. C. Paixão and C. E. Banks, *Microchim. Acta*, 2024, **191**, 1–12.
62 T. P. Lisboa, L. V. de Faria, W. B. V. de Oliveira, R. S. Oliveira, C. C. de Souza, M. A. C. Matos, R. M. Dornellas and R. C. Matos, *Anal. Bioanal. Chem.*, 2024, **416**, 215–226.
63 P. Clares, C. Pérez-Ràfols, N. Serrano and J. M. Díaz-Cruz, *Chemosensors*, 2022, **10**, 95.
64 L. C. Oliveira, D. S. Rocha, H. A. Silva-Neto, T. A. C. Silva and W. K. T. Coltro, *Microchim. Acta*, 2023, **190**, 1–11.
65 F. Pena-Pereira, W. Wojnowski and M. Tobiszewski, *Anal. Chem.*, 2020, **92**, 10076–10082.